J. Fluid Mech. (2017), *vol.* 816, R2, doi:10.1017/jfm.2017.112

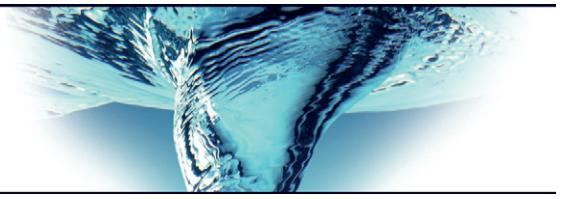

JFM RAPIDS
journals.cambridge.org/rapids

Restricted Euler dynamics along trajectories of small inertial particles in turbulence

Perry L. Johnson[1],† **and Charles Meneveau**[1]

[1]Department of Mechanical Engineering and Center for Environmental and Applied Fluid Mechanics, The Johns Hopkins University, Baltimore, MD 21218, USA

(Received 10 January 2017; revised 13 February 2017; accepted 14 February 2017; first published online 6 March 2017)

The fate of small particles in turbulent flows depends strongly on the velocity gradient properties of the surrounding fluid, such as rotation and strain rates. For non-inertial (fluid) particles, the restricted Euler model provides a simple low-dimensional dynamical system representation of Lagrangian evolution of velocity gradients in fluid turbulence, at least for short times. Here, we derive a new restricted Euler dynamical system for the velocity gradient evolution of inertial particles, such as solid particles in a gas, or droplets and bubbles in turbulent liquid flows. The model is derived in the limit of small (sub-Kolmogorov-scale) particles and low Stokes number. The system exhibits interesting fixed points, stability and invariant properties. Comparisons with data from direct numerical simulations show that the model predicts realistic trends such as the tendency of increased straining over rotation along heavy particle trajectories and, for light particles such as bubbles, the tendency of reduced self-stretching of the strain rate.

Key words: multiphase and particle-laden flows, turbulence theory, turbulent flows

1. Introduction

Small particles embedded in a turbulent flow have interesting behaviours when the particle density, ρ_p, is different from the density of the surrounding fluid, ρ_f. For example, within a certain parameter range, heavy particles tend to cluster in regions where the strain rate is higher than the rotation rate (Maxey 1987; Wang & Maxey 1993*a*; Eaton & Fessler 1994; Monchaux, Bourgoin & Cartellier 2012), while the opposite is true of lighter particles (Biferale, Scagliarini & Toschi 2010) such as bubbles (Wang & Maxey 1993*b*; Calzavarini *et al.* 2008) and oil droplets (Gopalan, Malkiel & Katz 2008). This clustering effect (Balkovsky, Falkovich & Fouxon 2001; Bec 2003) can enhance collision rates (Sundaram & Collins 1997; Reade & Collins 2000; Wang, Wexler & Zhou 2000; Falkovich, Fouxon & Stepanov 2002; Bewley, Saw & Bodenschatz 2013). The rate of clustering can be related to the velocity gradient

† Email address for correspondence: pjohns86@jhu.edu

structure of the surrounding fluid experienced by particles along their trajectories (Maxey 1987; Balkovsky *et al.* 2001). Other important aspects of multiphase flows in various applications, such as particle rotation and orientation (Pumir & Wilkinson 2011; Parsa *et al.* 2012; Chevillard & Meneveau 2013), droplet or bubble deformation (Maffettone & Minale 1998; Biferale, Meneveau & Verzicco 2014) and nutrient uptake (Batchelor 1980; Karp-Boss, Boss & Jumars 1996), similarly depend on the local velocity gradient structure. Much of the recent research on particle evolution in fluid turbulence (Toschi & Bodenschatz 2009) is based on direct numerical simulations (DNS). However, the high dimensionality of the Navier–Stokes equations especially for high-Reynolds-number turbulence (Ishihara, Gotoh & Kaneda 2009; Ireland, Bragg & Collins 2016) complicates basic analysis and the development of physical insights.

Dynamical systems models for the velocity gradient along Lagrangian paths provide an interesting possibility for reducing turbulent dynamics to a low-dimensional representation. Vieillefosse (1982, 1984) and Cantwell (1992) developed and studied the so-called restricted Euler system, which is obtained by taking the spatial gradient of the Navier–Stokes equations and neglecting the viscous and anisotropic pressure Hessian contributions. The model consists of a system of 3×3 nonlinear coupled ordinary differential equations for velocity gradient tensor elements,

$$\frac{\mathrm{D}A_{ij}}{\mathrm{D}t} = -A_{ik}A_{kj} + \frac{1}{3}A_{k\ell}A_{\ell k}\delta_{ij}, \quad i,j = 1,2,3, \tag{1.1}$$

where $A_{ij} = \partial u_i/\partial x_j$ is the fluid velocity gradient, $u_i(\boldsymbol{x}, t)$ is the velocity field and $\mathrm{D}/\mathrm{D}t = \partial/\partial t + u_k\partial/\partial x_k$ represents the Lagrangian time derivative following a fluid element in the flow.

The restricted Euler system can be projected to just two degrees of freedom and was shown to display important features seen in turbulent flows, such as the preferential alignment of the vorticity vector in the direction of the eigenvector associated with the median eigenvalue of the strain rate (Kerr 1985; Ashurst *et al.* 1987), negative skewness in longitudinal velocity gradients, as well as the tendency to produce extreme velocity gradient events (Meneveau 2011), which are clustered along the Vieillefosse tail. Without the neglected unclosed terms, however, the restricted Euler system eventually yields finite-time singularities for almost all initial conditions. The restricted Euler system played an important role in motivating subsequent work on modelling the unclosed terms (Girimaji & Pope 1990; Jeong & Girimaji 2003; Chevillard & Meneveau 2006; Biferale *et al.* 2007; Chevillard *et al.* 2008; Wilczek & Meneveau 2014; Johnson & Meneveau 2016) and related work on the perceived velocity gradient (Chertkov, Pumir & Shraiman 1999; Pumir, Bodenschatz & Xu 2013) at various scales, which has resulted in models capable of reproducing certain turbulent statistics with good quantitative accuracy, although extension to arbitrarily high Reynolds numbers remains an open challenge (Martins Afonso & Meneveau 2010; Meneveau 2011).

In this paper, we derive an extension to the restricted Euler system that considers the effect of inertia on the velocity gradient dynamics when following an inertial particle, yet can likewise be projected into a dynamical system with just two degrees of freedom, namely the two tensor invariants $Q = -(1/2)\mathrm{Tr}(\boldsymbol{A}^2)$ and $R = -(1/3)\mathrm{Tr}(\boldsymbol{A}^3)$. We explore whether the behaviour in the full RQ plane observed in DNS (Benzi *et al.* 2009) can be explained by the new model. The model is developed from governing equations in § 2, followed by an exploration of its behaviour compared with DNS in § 3. Model properties such as fixed points and stability are investigated analytically in § 4, before conclusions are drawn in § 5.

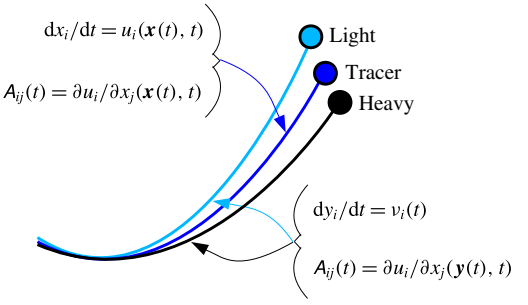

FIGURE 1. Sketch of the fluid and inertial particle trajectories. In this paper, we consider the time history of fluid velocity gradients, $A_{ij}(t)$, along these trajectories.

2. Model construction

As illustrated in figure 1, while fluid tracers (position $\boldsymbol{x}(t)$) move according to $\mathrm{d}x_i/\mathrm{d}t = u_i(\boldsymbol{x}, t)$, inertial particle trajectories ($\boldsymbol{y}(t)$) evolve following the particle velocity $\boldsymbol{v}(t)$ according to $\mathrm{d}y_i/\mathrm{d}t = v_i(t)$, where, in general, $v_i(t) \neq u_i(\boldsymbol{y}, t)$. When the particle radius $a \ll \eta = \nu^{3/4}\langle\epsilon\rangle^{-1/4}$ (η is the Kolmogorov length scale, where ν is the kinematic viscosity of the surrounding fluid and $\langle\epsilon\rangle$ is the average dissipation rate of the fluid flow) and $Re_a = a|\boldsymbol{v} - \boldsymbol{u}|/\nu \ll 1$ (particle Reynolds number), the dynamical equation of the inertial particle trajectory (Maxey & Riley 1983) in the absence of gravitational settling can be simplified to (Maxey 1987; Balkovsky *et al.* 2001)

$$\frac{\mathrm{d}v_i}{\mathrm{d}t} = \beta\frac{\mathrm{D}u_i}{\mathrm{D}t} + \frac{u_i - v_i}{\tau_p}, \tag{2.1}$$

where $\beta = 3\rho_f/(2\rho_p + \rho_f)$ is the added mass parameter and $\tau_p = a^2/3\nu\beta$ is the relaxation time for the trajectory of a spherical particle of radius a. For small Stokes number based on the Kolmogorov time scale ($\tau_\eta = \nu^{1/2}\langle\epsilon\rangle^{-1/2}$), $St = \tau_p/\tau_\eta \ll 1$, Maxey (1987) constructed a perturbation solution to linear order in St which yields the following approximation:

$$v_i = u_i - (1 - \beta)\tau_p\frac{\mathrm{D}u_i}{\mathrm{D}t}. \tag{2.2}$$

This solution admits an interpretation in terms of a particle velocity field, $v_i(\boldsymbol{x}, t)$, such that the velocity of a particle at location $y_i(t)$ can be approximated by $v_i(t) = v_i(\boldsymbol{y}(t), t)$. In this way, the time derivative of the particle can be interpreted as $\mathrm{d}/\mathrm{d}t = \partial/\partial t + v_k\partial/\partial x_k$. While at finite Stokes number the particle velocity field could be multi-valued as two particles can have different velocities at the same point, the linear perturbation expansion for $St \ll 1$ gives a single-valued particle velocity field. Since this velocity field has non-zero divergence, it can describe clustering effects due to particle inertia.

In this paper, we consider the evolution of the fluid velocity gradient, $A_{ij} = \partial u_i/\partial x_j$, along the particle trajectory, as sketched in figure 1. Considering a particle velocity field $v_i(\boldsymbol{x}, t)$, the evolution equation for the velocity gradient can be related to the Lagrangian evolution by $\mathrm{d}A_{ij}/\mathrm{d}t = \mathrm{D}A_{ij}/\mathrm{D}t + (v_k - u_k)\partial A_{ij}/\partial x_k$, which upon substitution of the gradient of Navier–Stokes yields

$$\frac{\mathrm{d}A_{ij}}{\mathrm{d}t} = -A_{ik}A_{kj} - \frac{\partial^2 p}{\partial x_i\partial x_j} - \frac{\partial v_k}{\partial x_k}A_{ij} - \frac{\partial T_{ijk}}{\partial x_k}, \tag{2.3}$$

where p is the pressure divided by density and T_{ijk} represents spatial fluxes of velocity gradient due to viscosity and inertial effects according to $T_{ijk} = -\nu\partial A_{ij}/\partial x_k + A_{ij}(1-\beta)\tau_p \mathrm{D}u_k/\mathrm{D}t$. A key step is to evaluate the divergence of the particle velocity field using (2.2) for a divergence-free fluid velocity field (Balkovsky *et al.* 2001), i.e. $\partial v_k/\partial x_k = -(1-\beta)\tau_p A_{k\ell}A_{\ell k}$. The final steps in deriving the new inertial restricted Euler system are, similarly to the classical restricted Euler model, (i) to replace the pressure Hessian $\partial_i\partial_j p$ by its isotropic part $\nabla^2 p\,(\delta_{ij}/3)$ and to invoke the pressure Poisson equation $\nabla^2 p = -A_{k\ell}A_{\ell k}$ and (ii) to neglect any spatial fluxes, i.e. set $T_{ijk} = 0$, where we make the strong assumption of neglecting fluxes due to viscosity and inertia effects.

The resulting system reads as follows:

$$\frac{\mathrm{d}A_{ij}}{\mathrm{d}t} = -A_{ik}A_{kj} + \frac{1}{3}A_{k\ell}A_{\ell k}\delta_{ij} + (1-\beta)\tau_p A_{k\ell}A_{\ell k}A_{ij}, \tag{2.4}$$

thus extending the restricted Euler system of equations to include inertial trajectory effects. The original restricted Euler equation is recovered by considering particles with equal density to the surrounding fluid, $\rho_p = \rho_f$, hence $\beta = 1$. Equation (2.4) thus shows, within the limitations of the restricted Euler assumptions, how the inertia of a particle impacts the rate of change for each of the velocity gradient components it experiences along its trajectory. It is important to note that the effect of viscosity essential to studying inertial particles, Stokes drag, is represented in (2.4), while the less crucial effect of spatial diffusion of fluid velocity gradient is neglected. These simplifications enable us to focus on the terms that can be represented exactly in a low-dimensional dynamical system.

The inertial restricted Euler dynamics given by (2.4) can be projected into the two-dimensional space of tensor invariants Q and R, and yields the following two-dimensional dynamical system:

$$\frac{\mathrm{d}Q}{\mathrm{d}t} = -3R - \frac{2}{3}\alpha Q^2, \quad \frac{\mathrm{d}R}{\mathrm{d}t} = \frac{2}{3}Q^2 - \alpha QR, \tag{2.5a,b}$$

where $\alpha = 6(1-\beta)\tau_p$ is the time scale representing inertial effects. The second invariant, $Q = (\Omega_{ij}\Omega_{ij} - S_{ij}S_{ij})/2$, represents the relative balance between local rotation, $\Omega_{ij} = (A_{ij} - A_{ji})/2 = -\epsilon_{ijk}\omega_k/2$, and straining, $S_{ij} = (A_{ij} + A_{ji})/2$. The third invariant, $R = -S_{ij}S_{jk}S_{ki}/3 - \omega_i S_{ij}\omega_j/4$, represents the balance between strain production and enstrophy production (Tsinober 2001).

For particles that are heavier than the surrounding fluid, $0 < \beta < 1$ and $\alpha > 0$. For particles lighter than the surrounding fluid, $1 < \beta < 3$ and $\alpha < 0$. For heavy particles ($\alpha > 0$), the inertial term in the evolution equation for Q tends to oppose rotation-dominant states ($Q > 0$) and reinforce strain-dominant states ($Q < 0$). The exact opposite is true for light particles, where the inertial term opposes highly straining states and favours highly rotating states. In this way, heavy particles cluster in straining regions ($Q < 0$) and lighter particles cluster in rotating regions ($Q > 0$), qualitatively mimicking well-known preferential concentration trends. In homogeneous turbulence, $\langle Q\rangle = 0$ and $\langle R\rangle = 0$, where angle brackets denote ensemble averaging (Betchov 1956), but when averaging over inertial trajectory ensembles, one observes that $\langle Q\rangle < 0$ for heavy particles and $\langle Q\rangle > 0$ for light particles (Ireland *et al.* 2016). The qualitative features of RQ space are sketched in figure 2, including this qualitative effect of inertia on $\langle Q\rangle$, which is valid for any random velocity field, but in (2.5) is combined with turbulence-like dynamics in a manner consistent with first principles.

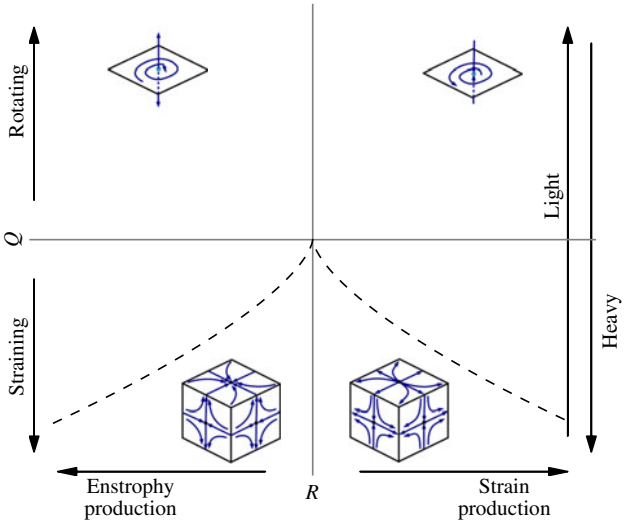

FIGURE 2. Sketch outlining the features of the RQ invariant space, including representative local flow topology cubes. The Vieillefosse tail (dashed line) represents the boundary between real and complex eigenvalues of the velocity gradient tensor.

3. Results

We now pursue a more detailed exploration of inertial effects in Navier–Stokes turbulence according to the restricted Euler model developed in § 2. Figure 3 shows the RQ phase-space portrait for non-inertial (fluid tracer), heavy and light particles computed numerically from (2.5). Also shown is the stationary joint probability density function (PDF) of Q and R computed from DNS at $Re_\lambda = 185$ (Bec *et al.* 2010). Although statistical stationarity (and hence direct comparison of the joint PDF) cannot be achieved in the system of (2.5) without introducing models for the neglected terms, the qualitative comparison of streamlines with the joint PDF in RQ space for heavy particles from DNS is informative. In particular, (*a*) shows the original restricted Euler system ($\alpha = 0$), for which trajectories move from left to right along lines of constant $Q^3 + (27/4)R^2$, eventually proceeding towards the finite-time singularity in the fourth quadrant (Vieillefosse 1982, 1984; Cantwell 1992). The sheared teardrop shape in the joint PDF in (*b*) highlights the dynamical significance of the Vieillefosse tail for the full (Navier–Stokes) dynamics of the velocity gradient tensor (Soria *et al.* 1994; Blackburn, Mansour & Cantwell 1996; Chong *et al.* 1998; Ooi *et al.* 1999).

In figure 3(*c*,*d*), the inertial restricted Euler phase-space portrait is shown for the case of heavy particles ($\alpha > 0$). The finite-time singularity down the Vieillefosse line in the fourth quadrant remains and is strengthened. In addition, some initial conditions proceed to a finite-time singularity down the other branch of the Vieillefosse line in the third quadrant. However, it is a very unstable manifold in the third quadrant, meaning that any noise in the system will prevent particles from proceeding to that singularity. In the first quadrant, the downward 'flow' of particles is enhanced while the left-to-right 'flow' is suppressed. The DNS results for heavy particles indeed show the tendency down the Vieillefosse tail in the fourth quadrant, as well as reduced probabilities in the upper half ($Q > 0$).

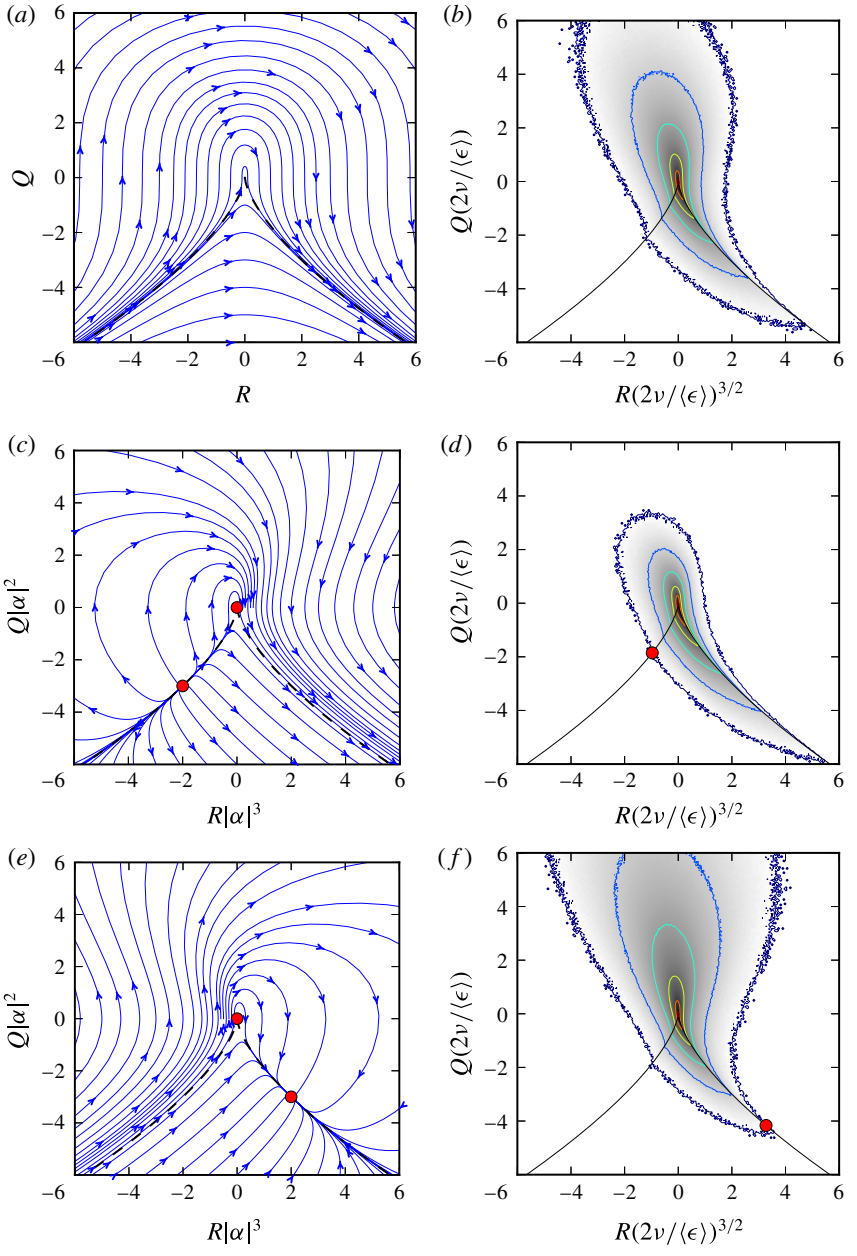

FIGURE 3. Restricted Euler streamlines (*a*,*c*,*e*) and DNS-computed joint PDF isocontours (*b*,*d*,*f*) for Lagrangian trajectories (*a*,*b*), heavy-particle trajectories with $\beta = 0$, $St = 0.3$, $\alpha = 1.8\sqrt{\nu/\langle\epsilon\rangle}$ (*c*,*d*) and light-particle trajectories with $\beta = 3$, $St = 0.1$, $\alpha = -1.2\sqrt{\nu/\langle\epsilon\rangle}$ (*e*,*f*). The time scale $|\alpha|$ is used to normalize the axes on the streamline plots, while $\sqrt{2\nu/\langle\epsilon\rangle}$ is used to normalize the axes for the DNS results, where $\langle\epsilon\rangle$ is the average turbulent dissipation rate from the simulation. The red circles show fixed points of the RQ dynamics, providing a visual connection between the two normalizations. The DNS data are from a pseudo-spectral simulation performed at $Re_\lambda = 185$ with a grid resolution of 512^3 (Bec *et al.* 2010). The PDF isocontours are spaced logarithmically with levels 10^z, $z = 1, 0, -1, -2, -3, -4$.

Finally, the phase-space trajectories for light particles ($\alpha < 0$) are shown in figure 3(e,f). The restricted Euler trajectories tend to proceed towards the fixed point in the fourth quadrant. There, a rapid collapse towards the Vieillefosse tail is followed by slower evolution along it towards the fixed point. The restricted Euler dynamics imposes more resistance to (e.g. noise-driven) movement away from the tail than movement along the tail. Trajectories no longer exhibit a finite-time singularity down the Vieillefosse tail. However, some trajectories in the second and third quadrants (e.g. $R(0)|\alpha|^3 < -3.2$ with $Q(0)|\alpha|^2 = 0$) do blow up in finite time with $Q > 0$ along inverted Vieillefosse-like manifolds with $Q \sim R^{2/3}$. The joint PDF from DNS data indeed suggests that the Viellefosse tail is still dynamically important for light particles, but that light particles do not tend to reach extreme states as far down the Viellefosse tail compared with neutral and heavy particles, an effect that may be qualitatively linked to the fixed point in the restricted Euler dynamics. The fixed point here takes on a clear physical interpretation, that inertial effects prevent light particles from sampling regions of the flow with more extreme values down the Vieillefosse tail. In general, the lower probabilities in the $Q < 0$ region are offset by higher probabilities in the $Q > 0$ region. Additionally, the upward and left-to-right movement in the first quadrant (towards $R \gg 0$) of the inertial restricted Euler streamlines is consistent with the enhanced probabilities observed in the DNS results.

While the qualitative comparisons between streamlines of the inertial restricted Euler system and joint PDFs from DNS are encouraging for both heavy and light particles, quantitative comparison of stationary statistics cannot be accomplished without models for the neglected unclosed terms, as was also the case for the original restricted Euler system (Meneveau 2011). Besides the pressure Hessian and viscous Laplacian, additional modelling work is probably necessary for the additional terms introduced for inertial trajectories, namely $\partial[(v_i - u_i)A_{ij}]/\partial x_k$. It is important to note that the finite-time singularities in the original and inertial restricted Euler systems are not physical and exist only because of the absence of the neglected terms.

The St numbers used in figure 3 are evidently low enough for good qualitative agreement, and increasing accuracy of the linear perturbation solution with further decreasing St could be further investigated with the careful development of reliable statistical closure schemes for the neglected terms to enable quantitative comparisons. For larger St (or larger $|\alpha|$), the model predicts that the equilibrium points will move ever closer to the origin, thus increasing the deviations of the joint PDF with those along tracer particles. This can be appreciated by comparing with the DNS of Benzi *et al.* (2009), which were for larger St than the present results.

4. Analysis

Due to its inherent simplicity, many of the features of the inertial restricted Euler system can be investigated analytically. A salient feature of the original restricted Euler equation ($\alpha = 0$) is the invariant $Q^3 + (27/4)R^2$ (Vieillefosse 1982; Cantwell 1992). For the extended system given by (2.5),

$$\frac{\mathrm{d}}{\mathrm{d}t}\left(Q^3 + \frac{27}{4}R^2\right) = -2\alpha Q\left(Q^3 + \frac{27}{4}R^2\right), \tag{4.1}$$

so that for the particular choice $Q^3 + (27/4)R^2 = 0$, this remains an invariant of the dynamics. Strikingly, this means that the Vieillefosse tail, $Q_v(R) = -(27/4)^{1/3}R^{2/3}$, is

an invariant manifold for all values of α, an important observation clearly supported by the DNS evidence in figure 3.

It is straightforward to show that (2.5) has two fixed points, one at the origin and another at $R_0 = -2/\alpha^3$, $Q_0 = -3/\alpha^2$, which lies on the Vieillefosse tail, i.e. $Q_0^3 + (27/4)R_0^2 = 0$, as clearly seen in figure 3. Linear stability analysis of this fixed point reveals eigenvalues of $\lambda_1 = 6/\alpha$ and $\lambda_2 = 1/\alpha$ with (unnormalized) eigenvectors $\boldsymbol{e}^{(1)} = (1, -(3/2)\alpha)^T$ and $\boldsymbol{e}^{(2)} = (1, \alpha)^T$. The fixed point is unstable for heavy particles and stable for light particles, as seen in figure 3. The slope of the Vieillefosse tail at the fixed point is $\mathrm{d}Q_v/\mathrm{d}R|_{Q_0} = \alpha$, so that the eigenvector associated with the more weakly stable/unstable eigenvector points along the Vieillefosse manifold.

Along the Vieillefosse manifold, the dynamics is given by $\mathrm{d}R/\mathrm{d}t = (3/2^{1/3})R^{4/3} + (3/2^{2/3})\alpha R^{5/3}$, which for $\alpha \neq 0$ can be written as

$$\frac{\mathrm{d}R}{\mathrm{d}t} = \frac{6}{\alpha^4}\left[\left(\frac{R}{R_0}\right)^{4/3} - \left(\frac{R}{R_0}\right)^{5/3}\right]. \tag{4.2}$$

This shows the reinforcement of the original finite-time singularity behaviour in the fourth quadrant for heavy particles as well as a similar path to singularity in the third quadrant, for $R < R_0 < 0$. It also shows that there is no longer a finite-time singularity along the Vieillefosse manifold for light particles due to the stable fixed point. This stable fixed point for light particles highlights the role of inertia in counteracting the tendency towards more heavily strain-dominated regions down the Vieillefosse tail. This tendency, meanwhile, is strengthened for heavy particles.

The linear stability of the Vieillefosse manifold is examined by considering the trajectory $Q(R) = Q_v(R) + \epsilon(R)$. Using $\mathrm{d}\ln\epsilon/\mathrm{d}t = \mathrm{d}\ln\epsilon/\mathrm{d}R\,\mathrm{d}R/\mathrm{d}t$, the linearized behaviour of ϵ can be shown to be

$$\frac{\mathrm{d}\ln\epsilon}{\mathrm{d}t} = 2^{1/3}\alpha R^{1/3}\left(R^{1/3} - \left(\frac{16}{\alpha^3}\right)^{1/3}\right). \tag{4.3}$$

When $\mathrm{d}\ln\epsilon/\mathrm{d}t > 0$, the Vieillefosse line is an unstable manifold. When $\mathrm{d}\ln\epsilon/\mathrm{d}t < 0$, it is a stable manifold. The stability of the manifold changes sign twice, once at the origin, and also at the point

$$(R_s, Q_s) = \left(\frac{16}{\alpha^3}, -\frac{12}{\alpha^2}\right). \tag{4.4}$$

For $\alpha > 0$ (heavy particles), the Vieillefosse manifold is stable for $0 < R < R_s$, while it is unstable if $R < 0$ or $R > R_s$. Meanwhile, for $\alpha < 0$ (light particles), it is stable for $R < R_s$ or $R > 0$ and unstable for $R_s < R < 0$. The point of neutral stability, R_s, has an opposite sign to the fixed point, R_0, and is also eight times larger in magnitude. Thus, it is unlikely to be of much relevance to the stationary statistics at low St number, as shown in figure 3.

5. Conclusions

With only two degrees of freedom, the extension of the restricted Euler system for inertial particle paths yields qualitative agreement with basic trends seen from DNS in the RQ plane. The trends observed follow directly from first principles, i.e. from the 'self-stretching' properties of the nonlinear term in the Navier–Stokes and

particle transport equations, whose effects are elucidated here by neglecting all of the 'non-local' spatial flux terms. While the restricted Euler system cannot itself offer quantitative predictions in most cases, the qualitative success in representing basic inertial effects suggests that it can be a good starting point for developing more complete models for velocity gradients along inertial particle trajectories for applications such as preferential (fractal) concentration (Bec 2003; Bec *et al.* 2006; Esmaily-Moghadam & Mani 2016) of heavy and light anisotropic particles (Parsa *et al.* 2012; Chevillard & Meneveau 2013) and deformation of liquid droplets (Biferale *et al.* 2014) or bubbles.

Acknowledgements

The authors are very grateful to L. Biferale and F. Toschi for making their DNS simulation data available for the plots generated in figure 3. P.J. was supported by a National Science Foundation Graduate Research Fellowship Program under grant no. DGE-1232825. C.M.'s research was made possible by a grant from The Gulf of Mexico Research Initiative.

References

ASHURST, WM. T., KERSTEIN, A. R., KERR, R. M. & GIBSON, C. H. 1987 Alignment of vorticity and scalar gradient with strain rate in simulated Navier–Stokes turbulence. *Phys. Fluids* **30** (8), 2343–2353.

BALKOVSKY, E., FALKOVICH, G. & FOUXON, A. 2001 Intermittent distribution of inertial particles in turbulent flows. *Phys. Rev. Lett.* **86** (13), 2790–2793.

BATCHELOR, G. K. 1980 Mass transfer from small particles suspended in turbulent fluid. *J. Fluid Mech.* **98**, 609–623.

BEC, J. 2003 Fractal clustering of inertial particles in random flows. *Phys. Fluids* **15**, 81–84.

BEC, J., BIFERALE, L., BOFFETTA, G., CENCINI, M., MUSACCHIO, S. & TOSCHI, F. 2006 Lyapunov exponents of heavy particles in turbulence. *Phys. Fluids* **18**, 091702.

BEC, J., BIFERALE, L., LANOTTE, A. S., SCAGLIARINI, A. & TOSCHI, F. 2010 Turbulent pair dispersion of inertial particles. *J. Fluid Mech.* **645**, 497–528.

BENZI, R., BIFERALE, L., CALZAVARINI, E., LOHSE, D. & TOSCHI, F. 2009 Velocity-gradient statistics along particle trajectories in turbulent flows: the refined similarity hypothesis in the Lagrangian frame. *Phys. Rev.* E **80**, 1–6.

BETCHOV, R. 1956 An inequality concerning the production of vorticity in isotropic turbulence. *J. Fluid Mech.* **1** (05), 497–504.

BEWLEY, G. P., SAW, E. W. & BODENSCHATZ, E. 2013 Observation of the sling effect. *New J. Phys.* **15**, 083051.

BIFERALE, L., CHEVILLARD, L., MENEVEAU, C. & TOSCHI, F. 2007 Multiscale model of gradient evolution in turbulent flows. *Phys. Rev. Lett.* **98**, 25–28.

BIFERALE, L., MENEVEAU, C. & VERZICCO, R. 2014 Deformation statistics of sub-Kolmogorov-scale ellipsoidal neutrally buoyant drops in isotropic turbulence. *J. Fluid Mech.* **754**, 184–207.

BIFERALE, L., SCAGLIARINI, A. & TOSCHI, F. 2010 On the measurement of vortex filament lifetime statistics in turbulence. *Phys. Fluids* **22** (6), 065101.

BLACKBURN, H. M., MANSOUR, N. N. & CANTWELL, B. J. 1996 Topology of fine-scale motions in turbulent channel flow. *J. Fluid Mech.* **310**, 269.

CALZAVARINI, E., VAN DEN BERG, T. H., TOSCHI, F. & LOHSE, D. 2008 Quantifying microbubble clustering in turbulent flow from single-point measurements. *Phys. Fluids* **20**, 040702.

CANTWELL, B. J. 1992 Exact solution of a restricted Euler equation for the velocity gradient tensor. *Phys. Fluids* **4** (4), 782–793.

CHERTKOV, M., PUMIR, A. & SHRAIMAN, B. I. 1999 Lagrangian tetrad dynamics and the phenomenology of turbulence. *Phys. Fluids* **11** (8), 2394–2410.

CHEVILLARD, L. & MENEVEAU, C. 2006 Lagrangian dynamics and statistical geometric structure of turbulence. *Phys. Rev. Lett.* **97** (17), 174501.

CHEVILLARD, L. & MENEVEAU, C. 2013 Orientation dynamics of small, triaxial-ellipsoidal particles in isotropic turbulence. *J. Fluid Mech.* **737**, 571–596.

CHEVILLARD, L., MENEVEAU, C., BIFERALE, L. & TOSCHI, F. 2008 Modeling the pressure Hessian and viscous Laplacian in turbulence: comparisons with direct numerical simulation and implications on velocity gradient dynamics. *Phys. Fluids* **20** (10), 101504.

CHONG, M. S., SORIA, J., PERRY, A. E., CHACIN, J., CANTWELL, B. J. & NA, Y. 1998 Turbulence structures of wall-bounded shear flows found using DNS data. *J. Fluid Mech.* **357**, 225–247.

EATON, J. K. & FESSLER, J. R. 1994 Preferential concentration of particles by turbulence. *Intl J. Multiphase Flow* **20**, 169–209.

ESMAILY-MOGHADAM, M. & MANI, A. 2016 Analysis of the clustering of inertial particles in turbulent flows. *Phys. Rev. Fluids* **1** (8), 084202.

FALKOVICH, G., FOUXON, A. & STEPANOV, M. G. 2002 Acceleration of rain initiation by cloud turbulence. *Nature* **419**, 151–154.

GIRIMAJI, S. S. & POPE, S. B. 1990 A diffusion model for velocity gradients in turbulence. *Phys. Fluids* **2** (2), 242.

GOPALAN, B., MALKIEL, E. & KATZ, J. 2008 Experimental investigation of turbulent diffusion of slightly buoyant droplets in locally isotropic turbulence. *Phys. Fluids* **20** (9), 095102.

IRELAND, P. J., BRAGG, A. D. & COLLINS, L. R. 2016 The effect of Reynolds number on inertial particle dynamics in isotropic turbulence. Part 1. Simulations without gravitational effects. *J. Fluid Mech.* **796**, 659–711.

ISHIHARA, T., GOTOH, T. & KANEDA, Y. 2009 Study of high Reynolds number isotropic turbulence by direct numerical simulation. *Annu. Rev. Fluid Mech.* **41**, 165–180.

JEONG, E. & GIRIMAJI, S. S. 2003 Velocity-gradient dynamics in turbulence: effect of viscosity and forcing. *Theor. Comput. Fluid Dyn.* **16** (6), 421–432.

JOHNSON, P. L. & MENEVEAU, C. 2016 A closure for Lagrangian velocity gradient evolution in turbulence using recent deformation mapping of initially Gaussian fields. *J. Fluid Mech.* **804**, 387–419.

KARP-BOSS, L., BOSS, E. & JUMARS, P. A. 1996 Nutrient fluxes to planktonic osmotrophs in the presence of fluid motion. *Oceanography Mar. Biol.: An Annual Rev.* **34**, 71–107.

KERR, R. M. 1985 Higher-order derivative correlations and the alignment of small-scale structures in isotropic numerical turbulence. *J. Fluid Mech.* **153**, 31–58.

MAFFETTONE, P. L. & MINALE, M. 1998 Equation of change for ellipsoidal drops in viscous flow. *J. Non-Newtonian Fluid Mech.* **78** (2–3), 227–241.

MARTINS AFONSO, M. & MENEVEAU, C. 2010 Recent fluid deformation closure for velocity gradient tensor dynamics in turbulence: timescale effects and expansions. *Physica* D **239** (14), 1241–1250.

MAXEY, M. R. 1987 The gravitational settling of aerosol particles in homogeneous turbulence and random flow fields. *J. Fluid Mech.* **174**, 441.

MAXEY, M. R. & RILEY, J. J. 1983 Equation of motion for a small rigid sphere in a nonuniform flow. *Phys. Fluids* **26** (4), 883–889.

MENEVEAU, C. 2011 Lagrangian dynamics and models of the velocity gradient tensor in turbulent flows. *Annu. Rev. Fluid Mech.* **43**, 219–245.

MONCHAUX, R., BOURGOIN, M. & CARTELLIER, A. 2012 Analyzing preferential concentration and clustering of inertial particles in turbulence. *Intl J. Multiphase Flow* **40**, 1–18.

OOI, A., MARTIN, J., SORIA, J. & CHONG, M. S. 1999 A study of the evolution and characteristics of the invariants of the velocity-gradient tensor in isotropic turbulence. *J. Fluid Mech.* **381**, 141–174.

PARSA, S., CALZAVARINI, E., TOSCHI, F. & VOTH, G. A. 2012 Rotation rate of rods in turbulent fluid flow. *Phys. Rev. Lett.* **109**, 1–4.

PUMIR, A., BODENSCHATZ, E. & XU, H. 2013 Tetrahedron deformation and alignment of perceived vorticity and strain in a turbulent flow. *Phys. Fluids* **25**, 035101.

PUMIR, A. & WILKINSON, M. 2011 Orientation statistics of small particles in turbulence. *New J. Phys.* **13**, 093030.

READE, W. C. & COLLINS, L. R. 2000 Effect of preferential concentration on turbulent collision rates. *Phys. Fluids* **12**, 2530–2540.

SORIA, J., SONDERGAARD, R., CANTWELL, B. J., CHONG, M. S. & PERRY, A. E. 1994 A study of the fine-scale motions of incompressible time-developing mixing layers. *Phys. Fluids* **6**, 871.

SUNDARAM, S. & COLLINS, L. R. 1997 Collision statistics in an isotropic particle-laden turbulent suspension. Part 1. Direct numerical simulations. *J. Fluid Mech.* **335**, 75–109.

TOSCHI, F. & BODENSCHATZ, E. 2009 Lagrangian properties of particles in turbulence. *Annu. Rev. Fluid Mech.* **41** (1), 375–404.

TSINOBER, A. 2001 *An Informal Introduction to Turbulence*. Kluwer Academic.

VIEILLEFOSSE, P. 1982 Local interaction between vorticity and shear in a perfect incompressible fluid. *J. Phys.* **43**, 837–842.

VIEILLEFOSSE, P. 1984 Internal motion of a small element of fluid in an inviscid flow. *Physica* A **125**, 150–162.

WANG, L.-P. & MAXEY, M. R. 1993*a* Settling velocity and concentration distribution of heavy particles in homogeneous isotropic turbulence. *J. Fluid Mech.* **256**, 27–68.

WANG, L.-P. & MAXEY, M. R. 1993*b* The motion of microbubbles in a forced isotropic and homogeneous turbulence. *Appl. Sci. Res.* **51**, 291–296.

WANG, L.-P., WEXLER, A. S. & ZHOU, Y. 2000 Statistical mechanical description and modelling of turbulent collision of inertial particles. *J. Fluid Mech.* **415**, 117–153.

WILCZEK, M. & MENEVEAU, C. 2014 Pressure Hessian and viscous contributions to velocity gradient statistics based on Gaussian random fields. *J. Fluid Mech.* **756**, 191–225.